Sensors and Actuators B 181 (2013) 361–367

Contents lists available at SciVerse ScienceDirect

Sensors and Actuators B: Chemical

journal homepage: www.elsevier.com/locate/snb

Focused-ion-beam-fabricated Au/Ag multilayered nanorod array as SERS-active substrate for virus strain detection

Kundan Sivashanmugan[a], Jiunn-Der Liao[a,b,*], Jin-Wei You[a], Chao-Liang Wu[c,d]

[a] Department of Materials Science and Engineering, National Cheng Kung University, 1 University Road, Tainan 70101, Taiwan
[b] Center for Micro/Nano Science and Technology, National Cheng Kung University, 1 University Road, Tainan 70101, Taiwan
[c] Department of Biochemistry and Molecular Biology, National Cheng Kung University, 1 University Road, Tainan 70101, Taiwan
[d] Institute of Basic Medical Sciences, National Cheng Kung University, 1 University Road, Tainan 70101, Taiwan

ARTICLE INFO

Article history:
Received 8 November 2012
Received in revised form 16 January 2013
Accepted 18 January 2013
Available online 28 January 2013

Keywords:
Surface-enhanced Raman scattering
Focused ion beam
Multi-layered nanorod arrays
Enhancement factor
Influenza virus strains

ABSTRACT

A surface-enhanced Raman scattering (SERS) substrate was fabricated as well ordered Au/Ag multilayered nanorod arrays (*fib*Au/Ag_R_n, $n = 0$–4) via the focused ion beam technique for the detection of the influenza A virus strain. Since the shape, thickness, space between nanorods, and dimensions affect the performance of SERS, these factors were optimized before the fabrication of the substrate by varying the thickness of the Au layer (4 variables), Ag layer (3 variables), and their corresponding Ag/Au repeated layers. Au/Ag multilayers with the optimal thickness were used to fabricate the designed SERS substrate. The results indicate that Ag layer plays an important role in the improvement of SERS mechanism by inducing the electromagnetic effect at the Au surface. The as-prepared *fib*Au/Ag_R_n substrate serves as an excellent SERS substrate, even verified at a very low concentration using rhodamine 6G as a reference, e.g., it exhibited an enhancement factor ranging from 2.62×10^6 to 1.74×10^7 using the proposed SERS substrate. Furthermore, the influenza A virus strains (A/WSN/33 (H1N1), A/England/12/64 (H2N2), and A/Philippine/2/82 (H3N2)) could be well distinguished at a low concentration of 10^6 PFU/ml.

1. Introduction

Respiratory tract infections, acute diseases caused by the influenza virus, are a major public health concern. However, the accurate detection of influenza virus strains takes time and requires a considerable concentration of the virus [1,2]. Methods for the laboratory diagnosis of influenza include the immunofluoresence test, enzyme-linked immunosorbent assay (ELISA) [3], hemadsorption [4], and reverse transcriptase polymer chain reaction (PCR) [5]. They provide excellent sensitivity, enabling the detection of specific influenza diagnostics. However, particular labeling techniques are required, placing constraints on some potential applications. Compared to established analytical techniques such as ELISA and immunofluorescence, surface-enhanced Raman scattering (SERS) is an extremely sensitive and selective technique for detecting surface species. Most of the signal enhancement in SERS compared to conventional Raman is attributed to the large increase in the generated local electric field [6,7]. A strong Raman signal is generated when analyte molecules interact with a metal surface, i.e., a SERS-active substrate [8,9]. The principle of SERS can be generally explained by a combination of an electromagnetic mechanism that describes the surface electron movement in the substrate and a chemical mechanism that is related to the charge transfer between the substrate and the analyte molecules [10–14]. SERS-active substrates based on localized surface plasmon resonance (LSPR) have been restricted to the noble metals (e.g., Ag, Au, Cu) and transition metals (e.g., Pt, Pd, Ru, Rh, Fe, Co, Ni) [15–19]. Some metals in the form of nanoparticles (NPs) or nanostructures (NSs) may induce strong light scattering and an enhancement of the local electromagnetic field in the vicinity of NPs or NSs. Particularly large enhancements of the electromagnetic field, called hot spots, can be found between adjacent NPs or at the edge of an NS [20].

NPs and NSs are novel tools for detecting Raman-active species at the nanometer scale. SERS-active substrates can be obtained either by the solvent-cast deposition of colloidal NPs [19] or by lithography techniques such as electron beam lithography [21,22] and nano-indentation [23]. The fabrication methods create high-precision regular patterns. SERS-active substrates have been used to detect nucleoproteins, oligonucleotides, and viruses [23–26]. Most of the fabrication methods focus on achieving large enhancement factors, but have low reproducibility and high cost, and generally lack the requisite characteristics needed to make SERS a platform-enabling technology. In recent years, the present authors have made reproducible SERS-active substrates with Au nanorod

* Corresponding author at: Department of Materials Science and Engineering, National Cheng Kung University, 1 University Road, Tainan 70101, Taiwan.
Tel.: +886 6 2757575x62971; fax: +886 6 2346290.
E-mail address: jdliao@mail.ncku.edu.tw (J.-D. Liao).

0925-4005/$ – see front matter © 2013 Elsevier B.V. All rights reserved.
http://dx.doi.org/10.1016/j.snb.2013.01.035

Table 1
Description of *fib*Au/Ag_R$_n$ samples S_1–S_11[a]: average height of a nanorod (H), spacing (S), and diameter of nanorods (D).

Sample code	Variable embedded thickness of Au (nm)	Variable embedded thickness of Ag (nm)	Fixed thickness of Au (nm)	Fixed thickness of Ag (nm)	Heigth of Au/Ag NR (nm)	Spacing between two NR (nm)	Diameter of NR (nm)
S_1	20			70	170 ± 10	30 ± 5	170 ± 10
S_2	40			70	170 ± 10	30 ± 5	170 ± 10
S_3	60			70	170 ± 10	30 ± 5	170 ± 10
S_4	80			70	170 ± 10	30 ± 5	170 ± 10
S_5		50	20		170 ± 10	30 ± 5	170 ± 10
S_6		100	20		170 ± 10	30 ± 5	170 ± 10
S_7		150	20		170 ± 10	30 ± 5	170 ± 10
S_8			20	40	170 ± 10	30 ± 5	170 ± 10
S_9			20	40	170 ± 10	30 ± 5	170 ± 10
S_10			20	40	170 ± 10	30 ± 5	170 ± 10
S_11			20	40	170 ± 10	30 ± 5	170 ± 10

[a] Au sample S_0 was used for a reference model with height of NR ≈ 420 nm, diameter of NR ≈ 170 nm, and spacing between two NRs ≈ 30 nm.

(NR) arrays via focused-ion-beam (FIB) technology. Hexagon-shape Au NR array SERS substrates can induce a higher electromagnetic effect due to the availability of multiple edges and a small curvature [27]. However, the LSPR observed from local NRs and the induced lighting rod effect strongly depend on the NR shape and the spacing between NRs [28,29]. The optical and enhancement properties of SERS substrates have been found to be a plasmon resonant formation with novel geometries to enhance Raman signals. In the present study, the FIB method is employed to fabricate well ordered Au/Ag multilayered NR arrays with an embedded Au and Ag layer of various thicknesses. The number of repeated layers of NR arrays affects the detection of Raman-active species. Optimized NR arrays were applied to distinguish influenza A virus strains at very low concentrations.

2. Experimental methods

2.1. Fabrication of Au/Ag multilayered nanorod arrays'

An Au/Ag multilayered thin film was deposited onto polished single-crystal silicon (1 0 0) wafers primed with a 15-nm-thick adhesion layer of chromium by an electron beam evaporator (VT1-10CE, ULVAC, Taiwan). All the NR patterns were designed using CorelDRAW software. The designs were implemented by applying a focused gallium ion beam (SMI 3050, SII Nanotechnology, Japan). The pattern size was about 14 μm × 14 μm with beam conditions of 30 kV acceleration voltage with UFine, 0.07 μm depth, 10 pA aperture, 70 μs dwell time, +0.56 OL fine, and 8-image scale with 50% overlap. The size and dimensions of as-fabricated Au/Ag multilayered NR arrays, denoted as *fib*Au/Ag_R$_n$ (n = 0, 1, 2, 3, and 4; n is the repeated unit number of layers of Au/Ag), are given in Table 1.

The as-fabricates *fib*Au/Ag_R$_n$ samples S_0–S_11 were briefly illustrated in Fig. 1. The optimal layer thickness for *fib*Au/Ag_R$_n$ was kept ≈420 nm. Au NR arrays (with a thickness of ≈420 nm), denoted as *fib*Au (S_0) and illustrated in Fig. 1(a), were prepared as a model substrate for a comparison with others *fib*Au/Ag_R$_n$. In Fig. 1(b), for *fib*Au/Ag_R$_0$ samples S_1–S_4, the embedded Au thickness was changed while the Ag thickness was kept constant (70 nm); for *fib*Au/Ag_R$_0$ samples S_5–S_7, the embedded Ag thickness was changed while the Au thickness was kept constant (20 nm), as illustrated Fig. 1(c). The other samples were *fib*Au/Ag_R$_1$ (S_8), *fib*Au/Ag_R$_2$ (S_9), *fib*Au/Ag_R$_3$ (S_10), and *fib*Au/Ag_R$_4$ (S_11). Samples S_8–S_11 had one repeated unit with an Au thickness of 20 nm and an Ag thickness of 40 nm, as shown in Fig. 1(d) and described in Table 1. A field-emission scanning electron microscope (FE-SEM, JSM-7001, JEOL, Japan) was used to analyze the morphology of the as-prepared *fib*Au/Ag_R$_n$ substrates. The composition was examined by a high-resolution field-emission transmission electron microscope (HR-FETEM, JEM-2100F, JEOL, Japan) equipped with an energy-dispersive spectrometer (EDS) detector and operated at 200 kV. Samples for HR-FETEM analysis were prepared by using FIB and then placed onto carbon-coated Cu grids.

2.2. Molecular probes for the evaluation of enhancement factor

Rhodamine 6G (R6G, Sigma, Germany), used as the molecular probe, was diluted with phosphate-buffered saline (PBS, Sigma, Germany) solution to a concentration of 10^{-4} M. To verify the enhancement factor (EF) of *fib*Au/Ag_R$_n$, the substrate with the molecular-probe-containing solution was covered with a glass slide and then immediately measured using Raman spectroscopy. The Raman spectrum was taken by a confocal microscopy Raman spectrometer (inVia Raman Microscope, Renishaw, United Kingdom) using a He–Ne laser with excitation of 633 nm wavelength. An air-cooled CCD was used as the detector; the incident power was 3 mW. The *fib*Au/Ag_R$_n$ with the molecular-probe-containing solution was then scanned with an integration time of 10 s over an area of 1 μm × 1 μm (the size of the laser spot was ~1 μm), using a 50× objective. Before each batch, the Raman shift was calibrated using a signal of 520 cm^{-1} with the absolute intensity from a standard silicon wafer.

The EF measurement was estimated according to the standard equation [30]:

$$\mathrm{EF} = \frac{I_{\mathrm{sers}}}{I_{\mathrm{bulk}}} \times \frac{N_{\mathrm{bulk}}}{N_{\mathrm{sers}}} \quad (1)$$

where I_{sers} and I_{bulk} are SERS and normal Raman scattering intensities, respectively; N_{sers} and N_{bulk} are the numbers of molecules

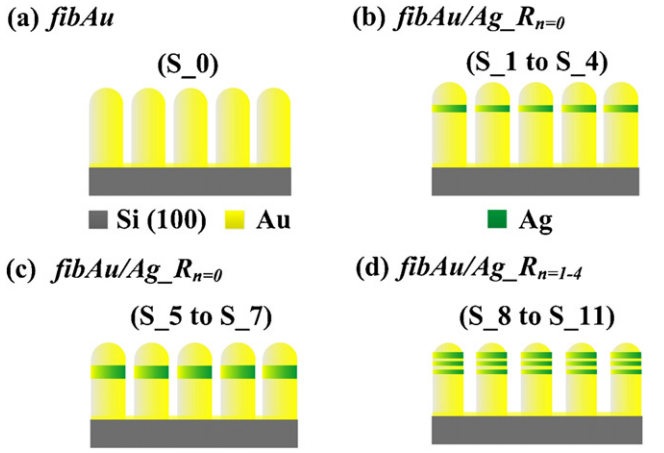

Fig. 1. Schematic illustrations of all *fib*Au/Ag_R$_n$ samples (as also described in Table 1: (a) *fib*Au (S_0), (b) *fib*Au/Ag_R$_0$ (S_1–S_4) with a constant Ag thickness, (c) *fib*Au/Ag_R$_0$ (S_5–S_7) with a constant Au thickness, and (d) *fib*Au/Ag_R$_1$ (S_8), *fib*Au/Ag_R$_2$ (S_9), *fib*Au/Ag_R$_3$ (S_10), and *fib*Au/Ag_R$_4$ (S_11) with one repeated unit (n = 1) of 20 nm Au and 40 nm Ag of thickness.